Feed-Forward and Feed-Backward Amplification Model from Cochlear Cytoarchitecture: An Interspecies Comparison

Yong-Jin Yoon,[†] Charles R. Steele,[†] and Sunil Puria[†‡*]
[†]Department of Mechanical Engineering and [‡]Department of Otolaryngology, Head and Neck Surgery, Stanford University, Stanford, California

ABSTRACT The high sensitivity and wide bandwidth of mammalian hearing are thought to derive from an active process involving the somatic and hair-bundle motility of the thousands of outer hair cells uniquely found in mammalian cochleae. To better understand this, a biophysical three-dimensional cochlear fluid model was developed for gerbil, chinchilla, cat, and human, featuring an active "push-pull" cochlear amplifier mechanism based on the cytoarchitecture of the organ of Corti and using the time-averaged Lagrangian method. Cochlear responses are simulated and compared with in vivo physiological measurements for the basilar membrane (BM) velocity, V_{BM}, frequency tuning of the BM vibration, and Q_{10} values representing the sharpness of the cochlear tuning curves. The V_{BM} simulation results for gerbil and chinchilla are consistent with in vivo cochlea measurements. Simulated mechanical tuning curves based on maintaining a constant V_{BM} value agree with neural-tuning threshold measurements better than those based on a constant displacement value, which implies that the inner hair cells are more sensitive to V_{BM} than to BM displacement. The Q_{10} values of the V_{BM} tuning curve agree well with those of cochlear neurons across species, and appear to be related in part to the width of the basilar membrane.

INTRODUCTION

It is well known that the cochlea of the inner ear transforms a sound signal input into a neural excitation output. Experiments have shown that for a fixed input frequency, a traveling wave on the basilar membrane (BM) builds to a peak at a certain point along the membrane and then rapidly decays beyond that point. The location of the peak depends on the frequency, so each location on the BM is said to have a "best frequency" (BF) associated with it that produces the maximum response amplitude at that point on the BM.

A sensory epithelium attached to the BM, called the organ of Corti (OC), contains sensory hair cells which respond to the BM motion and initiate neural excitation. Three rows of outer hair cells (OHCs) most likely use a piezoelectriclike mechanism to provide an amplification of the wave for low input amplitudes, an effect that is known as the active amplifier mechanism (1). The electromotile force of the OHCs has been shown to persist to >80 kHz (2). A large-scale model of the OC (3) emphasizes the spatial arrangement of its components. In particular, the apical inclination of the OHCs has been shown (4) to provide a spatial "feed-forward" effect that greatly enhances the wave amplitude near the BF. Such an approach has been utilized in one- (1-D), two- (2-D) (5,6), and three-dimensional (3-D) (7,8) fluid models. These models have a small number of parameters, each of which has a clear physical interpretation. However, the BM velocity simulation results from these models (7,8) disagree with in vivo measurements in showing 1), an excessive phase excursion and 2), a shift in the BF of around an octave for the passive and active conditions, instead of the measured half-octave shift. In recent work (9), it has been found that returning to the time-averaged Lagrangian used in (10) reduces the phase error.

Another prominent feature is an overlapping and repeating "Y"-shaped structure between the reticular lamina and basilar membrane as the base of each angled OHC connects with the base of the angled phalangeal process at the top of each supporting Deiters rod (Fig. 1). This Y-shaped structure leads to a framework for cochlear amplification in which the tilted OHCs provide a positive, "feed-forward" force on the BM (the "push") apically toward the helicotrema and the phalangeal processes provide a negative, "feed-backward" force (the "pull") basally toward the stapes (Fig. 1). The push and pull work together to provide an increase of two orders of magnitude in the amplitude of the wave for short wavelengths on the BM, but they cancel each other out for long wavelengths. For very short wavelengths above the BF, the viscosity of the fluid dominates. Thus, significant enhancement occurs for a narrow band of spatial wavelengths, without the need for special filtering or tuning of parameters at each BF.

The relationship between the BF, BM sensitivity, and BM sharpness of tuning is not well established. In this work, we elucidate the relationship between these quantities and the model inputs for the relatively low-frequency cochleae of human and chinchilla and the relatively high-frequency cochleae of cat and gerbil. Extensive BM measurements are available for one species in each group. The calculations for the simple box model of the cochlea with the push-pull mechanism and the time-averaged Lagrangian method yield results very similar to animal measurements of the BM

Submitted March 19, 2010, and accepted for publication November 16, 2010.

*Correspondence: puria@stanford.edu

Yong-Jin Yoon's present address is Department of Mechanical and Aerospace Engineering, Nanyang Technological University, Singapore, 639798, Singapore.

Editor: Arthur Sherman.

0006-3495/11/01/0001/10 $2.00

doi: 10.1016/j.bpj.2010.11.039

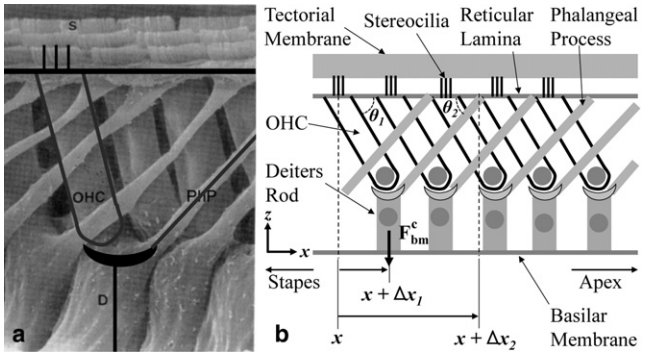

FIGURE 1 (*a*) Scanning electron micrograph of a longitudinal view of the organ of Corti of a mole rat cochlea (13), showing a representative OHC, Deiters rod (*D*), phalangeal process (*PhP*), and stereocilia bundle (*S*). (*b*) Schematic of the longitudinal view of the organ of Corti, showing the tilt of the OHCs based on the scanning electron micrograph. For one hair cell whose apex lies at a distance x, the base is located at distance $x + \Delta x_1$, whereas the phalangeal process connected to the base of the hair cell is attached to the reticular lamina at $x + \Delta x_2$. θ_1 is the OHC angle with respect to the reticular lamina, and θ_2 is the phalangeal process angle with respect to the reticular lamina. These structures form the repeating "Y"-shaped pattern. The force on the BM through the Deiters rod is F^c_{bm}, which, for the OHC whose apex is at x, consists of the downward push due to an expansion of the OHC at x and an upward pull through the phalangeal process due to an expansion of the OHC whose apex is at $x + \Delta x_2$.

velocity (V_{BM}) for gerbil (11) and chinchilla (12). In addition to the simulations of V_{BM}, BM isovibration and sharpness of cochlear tuning curves are calculated from the cochlear model presented here, and the model results are compared against measurements of BM vibration, auditory neural-tuning at thresholds, and tuning sharpness of cochlear neurons in animals, as well as predictions of auditory-nerve-fiber frequency-threshold curves (ANFTCs) in humans.

MATERIALS AND METHODS

Theoretical background

Overall features and dimensions of the 3-D hydrodynamic model used in this study are described in Fig. S1 of the Supporting Material. This is a standard "box" model of the cochlea with an asymptotic Wentzel-Kramers-Brillouin (WKB) solution method for the differential equations describing the mechanics of the cochlea. The full mathematical formulation for the passive model is described in the Supporting Material.

Electromotility of OHCs

Fig. 1 *a* shows a lateral view of the OC of a mole rat cochlea (13). Prominent are the rows of OHCs and phalangeal processes (PhPs). Each OHC is attached at its upper end to the reticular lamina, through which the stereocilia protrude. The lower portion contains Deiters cells, each of which contains a cup that attaches to an OHC and to a PhP that extends to the reticular lamina. Each cup is connected to the BM via a Deiters rod (*D*). Because of the attachment of the stereocilia to the overlying tectorial membrane, the total force acting on the BM (F_{BM}) causes a radial shear force on the stereocilia that opens transduction channels and causes a change in the OHC intracellular potential. Because of the electromotility of the OHC membrane (1), this causes a change in the length of the cell. A force toward the scala tympani, downward in Fig. 1, results in a depolarization and expansion of the OHC. Thus, a downward force on the BM causes an additional downward push from the OHC through the Deiters rod. It seems that the electromotility of the OHC would therefore only cause a decrease in the effective stiffness of the BM, which does not put additional energy into the dynamic response and thus does not amplify the BM motion. Consequently, many authors, beginning with Neely and Kim (14), have introduced various time-delay mechanisms for different purposes—to stabilize the negatively damped oscillators, for example (15)—but with scant physical justification. However, we follow the strong suggestion (3) that the spatial geometry has significance for cochlear amplification that needs to be explored.

The push-forward/pull-backward active model

Because of their angular orientations, each OHC connects to a PhP and Deiters rod to form a "Y"-shaped structure between the reticular lamina and the BM. As indicated in Fig. 1 *b*, a downward force on the BM at a distance x from the stapes causes a shear on the stereocilia at that point. Through the transduction process, the OHC expands, but because of the inclination of the OHC, the downward push on the BM occurs at the distance $x + \Delta x_1$. This is the "push-forward" or "positive feed-forward" effect.

The force of OHC expansion is equal and opposite at the cell ends. The cantilever arrangement of the reticular lamina and the tectorial membrane provides little resistance to this upward force, so all that remains to carry this force is the upper end of the PhP. In Fig. 1 *b*, the shear of the OHC at $x + \Delta x_2$ causes a tension in the PhP connected at that point and an upward force on D located at $x + \Delta x_1$. This is the "pull-backward" or "negative feed-backward" effect. Thus, the expansion of an OHC causes a downward push at a distance Δx_1 in the forward (apical) direction, and an upward pull at a distance $\Delta x_2 - \Delta x_1$ in the backward (basal) direction. There is also a ripple effect, extending in both directions, but we consider only the primary push and pull. Of course, for the response to a given frequency, all the quantities vary sinusoidally. However, it seems convenient to keep the "push-pull" designation.

The total force acting on the BM (F_{BM}) is twice the fluid force (F^f_{BM}), for fluid on both sides of the BM, plus the OHC force acting through the Deiters rods, F^C_{BM}:

$$F_{BM} = 2F^f_{BM} + F^C_{BM}. \tag{1}$$

The fluid force is the same as for the 3-D passive box model. For small amplitudes, the transduction and OHC motility are linear, so the cell force is proportional to the total force on the BM. Thus, the cell force acting on the BM at the point $x + \Delta x_1$ in Fig. 1 *b* depends on the total force on the BM at x and the total force acting on the BM at $x + \Delta x_2$, as expressed by the difference equation (9)

$$F^C_{BM}(x + \Delta x_1, t) = \alpha_1[F_{BM}(x,t)] - \alpha_2[F_{BM}(x + \Delta x_2, t)]\,. \tag{2}$$

The constants of proportionality, or "gains", from the OHC push and the PhP pull are α_1 and α_2, respectively. Because of the small resistance to vertical force of the reticular lamina and tectorial membrane, the net push and pull must be equal, so $\alpha_1 = \alpha_2 = \alpha$ is assumed. The details of the OHC compliance, transduction, somatic motility, and possibly stereociliary active mechanics are all lumped into the α gain, which is assumed to be independent of frequency.

With the WKB approximation, all quantities are in the form of an exponential multiplied by a slowly varying function,

$$F^C_{BM}(x,t) = e^{i\left[\omega t - \int_0^x n(x,\omega)dx\right]} F(x)\,, \tag{3}$$

in which ω is the frequency and $n(x,\omega)$ is the local wave number. With this, the spatial difference can be approximated as

$$F^C_{BM}(x + \Delta x_1, t) = F^C_{BM}(x,t)e^{-in\Delta x_1}. \quad (4)$$

This is valid when the (complex) wave number $n(x,\omega)$ does not change significantly in the distance Δx_1. Therefore, the relations Eq. 1 and Eq. 2 reduce to

$$F_{BM} = 2F^f_{BM} + F^C_{BM} = \frac{2F^f_{BM}}{1 - \alpha_1 e^{-in\Delta x_1} + \alpha_2 e^{-in(\Delta x_2 - \Delta x_1)}}. \quad (5)$$

Thus, the box model in Fig. S1 is used, with the elaborate OC in Fig. 1 represented by the simple terms in the denominator of Eq. 5.

The power series expansion of the denominator is

$$1 - \alpha e^{-in\Delta x_1} + \alpha e^{-in(\Delta x_2 - \Delta x_1)} = 1 - \alpha in\Delta x_2 + \ldots, \quad (6)$$

which shows that the feed-forward/backward effect is negligible for long wavelengths, when the magnitude of $n(x,\omega)$ is small. The wavelength is defined as $2\pi/n(x,\omega)$. Since the fluid loading in Eq. 5 is primarily masslike, the first effect for shorter wavelengths in Eq. 6 is "negative damping". For a reversed traveling wave, obtained by changing the sign of n, the effect is an increase in positive damping.

Matching the force from the fluid and the OHCs in Eq. 5 to the BM stiffness yields the eikonal (dispersion) relation. For a given frequency, this must be solved at each point for the wave number $n(x,\omega)$. A Newton-Raphson method is used, which generally works well. The full behavior is not transparent from Eq. 6, but can be seen from the numerical results. For modest values of the gain, $\alpha < 0.2$, the real part of n, which gives the phase, is little affected by the push-pull terms. The imaginary part of n can be substantially modified. Generally, the imaginary part of n is affected by the viscosity of the fluid and causes the rapid decrease in amplitude in the region past the maximum response (the BF). However, the push-pull terms in Eq. 6 can overcome the viscosity effect and produce a region near the BF where the sign of the imaginary part of n is reversed, i.e., a region of negative damping. Apically the fluid viscosity resumes dominance and the amplitude decreases exponentially. Thus, for a given frequency, the push-pull is negligible for long wavelengths (small real part of n) and very short wavelengths (large real part of n), but very significant for a band of wavelengths near the BF. This is an important attribute of the feed-forward and feed-backward model.

The push-pull model for the OC involves just the three parameters Δx_1, Δx_2, and α. Reasonable values for the distances Δx_1 and Δx_2 are used based on the OC cytoarchitecture, whereas the gain α is adjusted for a best fit with the experiments. In Lim and Steele (7), the saturation of the transduction is included by making α amplitude-dependent. From a theoretical consideration (2,16), it appears that transduction and motility of the OHCs are possible at high frequencies as well as at lower frequencies. A strong argument is made by Peng and Ricci (17) that both somatic motility of OHCs and active hair bundle mechanics are necessary for cochlear amplification. In this work, a gain that is independent of frequency and cochlear location was used.

The cochlear model was used to calculate the physiological responses of four mammalian cochleae (gerbil, chinchilla, cat, and human) including 1), BM velocity (V_{BM}), 2), BM isovelocity and isodisplacement tuning curves, and 3), sharpness of cochlear tuning curves. The input parameters were the nominal material properties listed in Table S1; the scala vestibuli area, BM width, and BM thickness as functions of distance from the stapes (Fig. 2); and the length of the cochlea, stapes footplate area (A_{st}), length of the OHCs (18), and fiber volume fraction (7) in Table S2, based on anatomical measurements for gerbils (19–22), chinchillas (23,24), cats (25–27), and humans (28–31).

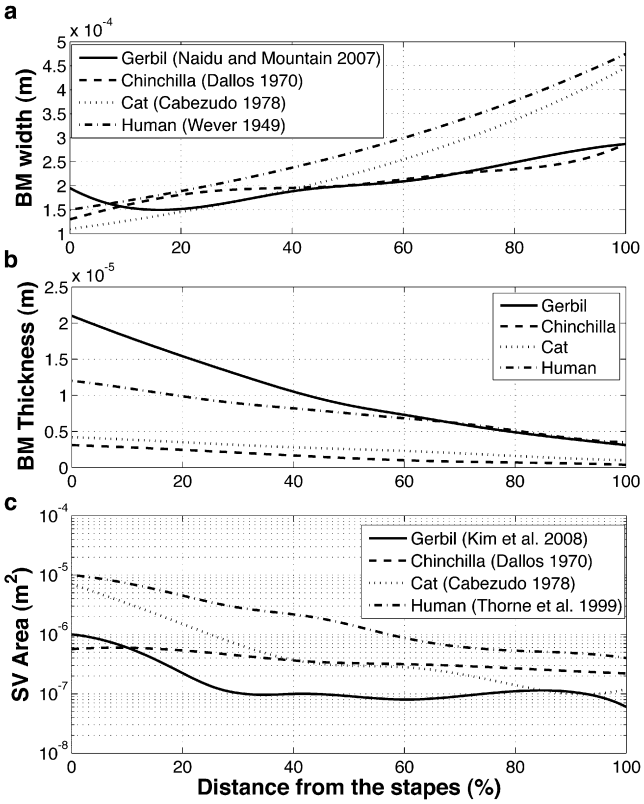

FIGURE 2 Dimensions of the BM width (*a*), BM thickness (*b*), and scala vestibuli (SV) area (*c*), for gerbils (*solid lines*), chinchillas (*dashed lines*), cats (*dotted lines*), and humans (*dash-dotted lines*) versus the distance from the stapes as a percentage of the total cochlear length. The gerbil BM thickness is taken not from a physical measurement, but from an equivalent flat plate.

Basilar membrane isovelocity and isodisplacement tuning curves

The model BM "isovelocity" and "isodisplacement" tuning curves (see Fig. 4) were calculated using neural-tuning threshold measurements for gerbil, chinchilla, and cat, and using psychophysical tuning-threshold measurements for human. For each threshold-measurement curve, the input pressure at the frequency with the minimum value (i.e., at the "characteristic", or "best", frequency) was used to determine, for the appropriate model, the corresponding BM velocity and displacement. The input sound pressure level (SPL) and α parameters for a given model were then iteratively computed for the other frequencies such that these BM velocity and displacement values were conserved. The resulting ensembles of input SPLs that yield the same BM velocity (or BM displacement) for a given model are then reported as the BM isovelocity (or isodisplacement) tuning curves.

RESULTS

BF-to-place map

The passive-model calculations of the BF versus place on the basilar membrane (i.e., the percentage of the total cochlea length, starting from the stapes) for four species (gerbil, chinchilla, cat, and human) are shown with their corresponding measurements in Fig. S2. The computed

and measured BF-to-place maps are in agreement within 5% for each species, except in the apical region of the cat cochlea, where the error is as large as 20% (Fig. S2).

Frequency response of the BM velocity (V_{BM})

The interspecies cochlear BM velocity (V_{BM}) computed relative to the stapes velocity (V_{ST}) (the relative BM velocity) is shown in terms of magnitude and phase in Fig. 3 for the passive and active cochlear models. The relative BM velocities of the gerbil and chinchilla cochlear models are compared with in vivo experimental data for gerbil (11) and chinchilla (12).

The relative BM velocities for the gerbil and chinchilla passive models (Fig. 3, *thin lines*) show qualitatively and quantitatively good magnitude and phase agreement with the animal measurements (Fig. 3, *open squares*), which were measured at a high stimulus level (SPL of 90–100 dB in the ear canal).

For the relative BM velocity in the active case, the push-pull active mechanism was added to the passive model, with the push-pull gain factor (α), the OHC angle (θ_1), and the phalangeal process angle (θ_2) included. Table 1 lists these additional parameters, as well as the best frequency and simulation location (x*), for the V_{BM} simulation of the interspecies cochlear models. The gerbil and chinchilla BM velocity simulations of the active model (Fig. 3, *thick lines*) also show good qualitative and quantitative agreement with the available data (Fig. 3, *asterisks*) at low stimulus levels (SPL of <40 dB at the ear canal), with peak gains of 48 and 76 dB (24 and 38 dB above the corresponding peaks for the passive condition) for gerbil and chinchilla, respectively (Fig. 3). Similar agreement was noted between the modeled and measured gerbil transfer functions of ear canal pressure to scala tympani pressure near the BM, for the active and passive cases (32) (Fig. S3).

TABLE 1 Parameters for the V_{BM} simulation

	Gerbil	Chinchilla	Cat	Human
Best frequency (BF) (kHz)	10	7	18	8
Distance from the stapes (x*) (mm)	4.2	4	5.4	6.4
OHC angle (θ_1)*	85° (37)	75°	85°	85°
Phalangeal process angle (θ_2)	30°	22°	25°	25°
Gain factor (α) for V_{BM}	0.11	0.11	0.11	0.11

Listed parameters are for the simulations in Fig. 3.
*The only reported measurement of the OHC angle θ_1 is for the gerbil (37).

In the relative BM velocity magnitude plot for the gerbil, the BF for the passive case (Fig. 3, *circles*) shifts from 10 kHz to 13 kHz, both in the simulation and in the experiment. Similar shifts in BF are seen for the other animals. This shift is sensitive to the phalangeal process angle (θ_2) for all species.

The relative BM velocity phase of the gerbil cochlea shows agreement with the measurement up to the BF location to within 70°, and the phase of the chinchilla cochlea

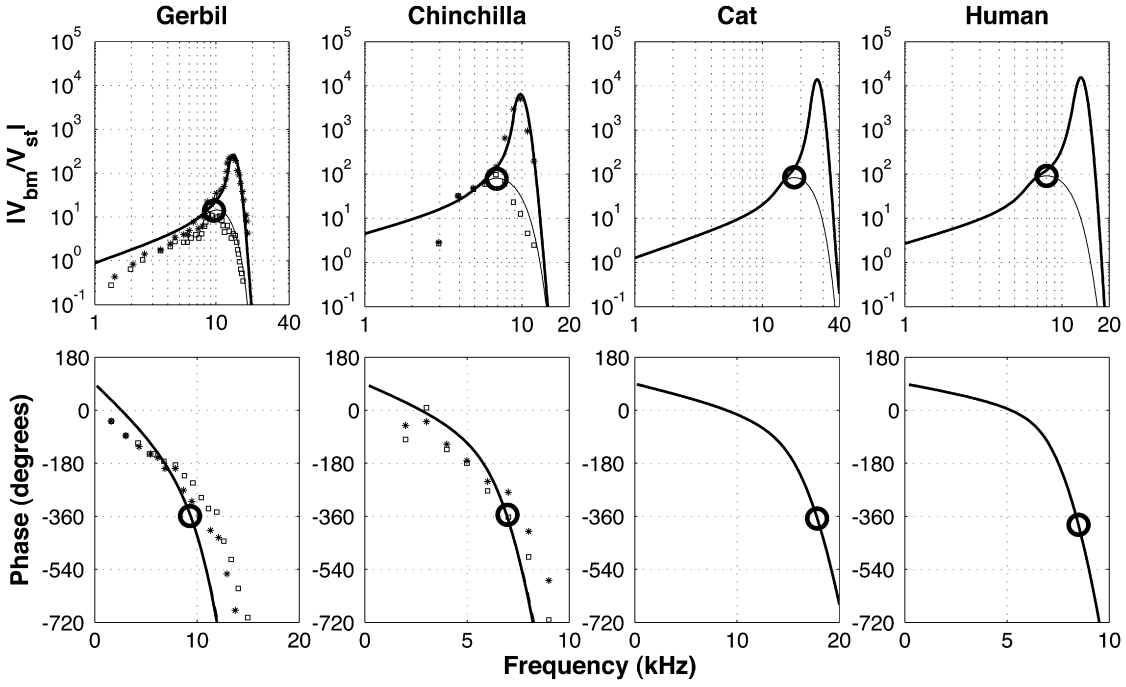

FIGURE 3 Passive (*light solid lines*) and active (*heavy solid lines*) models of basilar membrane velocity (V_{BM}) relative to stapes velocity (V_{ST}) magnitude (*upper row*) and corresponding phase (*lower row*) for the gerbil, chinchilla, cat, and human cochleae. Passive (*open squares*) and active (*asterisks*) experimental data are included for comparison with gerbil (100 dB SPL input for passive and 30–40 dB SPL for active) (11) and for chinchilla (90 dB SPL for passive and 10–20 dB SPL for active) (12). Thick black circles mark the BF corresponding to the passive case. Details of the simulation parameters are in Table 1.

shows agreement with the measurement over the entire frequency range to within 40°. Above the BF location (10 kHz), the phase of the gerbil BM velocity from the model shows a steeper roll-off than the phase from experiment, which corresponds to a higher wave number in the model above 10 kHz. The phase of the relative BM velocity in both the gerbil and chinchilla cochlear models shows a phase excursion of around one cycle near the BF location, which is also observed in the cat and human.

The similarity between the modeled and measured phase excursions using the model presented here is one of the most significant improvements provided by the time-averaged Lagrangian method, compared to the 2.5 and 3.5 cycles of phase excursion near the BF region using previous cochlear models for gerbil and chinchilla, respectively (7,8), which were the only animals tested.

BM vibration and neural tuning at threshold

In this study, the relationship between BM vibration and auditory neural thresholds is studied by comparing simulations of BM isovelocity and isodisplacement tuning curves using the current mathematical cochlear models to neural (or psychophysical) tuning curves at threshold for the four species (gerbil, chinchilla, cat, and human).

Fig. 4 shows the simulation of the BM isovibration tuning curves, along with the neural-tuning measurements from the four species. Neural tuning, BM isodisplacement, and BM isovelocity threshold measurements for a chinchilla cochlea (33) are shown, whereas for the other species only neural-tuning measurements (34,35) for gerbil and cat, and a psychophysical-tuning measurement (36) for human cochlea, are shown. For the chinchilla cochlea (Fib. 4 *b*), the BM isodisplacement and isovelocity tuning calculations are compared directly with the in vivo BM isodisplacement, BM isovelocity, and neural-tuning measurements.

TABLE 2 Parameters for the auditory neural threshold simulations

	Gerbil	Chinchilla	Cat	Human
Distance from the stapes (x*) (mm)	5.9	3.9	13.3	18.4
OHC angle (θ_1)	85° (37)	75°	75°	75°
Phalangeal process angle (θ_2)	30°	20°	20°	20°
Middle ear gain (dB SPL)	32	32	32	26

Simulation results are seen in Fig. 4.

Table 2 lists the parameters for the interspecies cochlear model that were used for the neural-tuning threshold simulations, including the distance from the stapes (x*), the angle of the OHCs (θ_1), the angle of the phalangeal processes (θ_2), and the middle-ear gain. Of the θ_1 angles listed in Table 2, the gerbil OHC angle was reported by Karavitaki (37), whereas the other values were merely estimated. The values for θ_2 were based on observations of the anatomy (3,13). In this model, the push-pull gain factors (α) were chosen according to the stimulus levels determined in the threshold experiments. Table 3 lists the values of α used for different input sound pressure ranges for the four species. For small stimulus levels, α is almost constant across species, and at its maximum value. As the stimulus level increases,

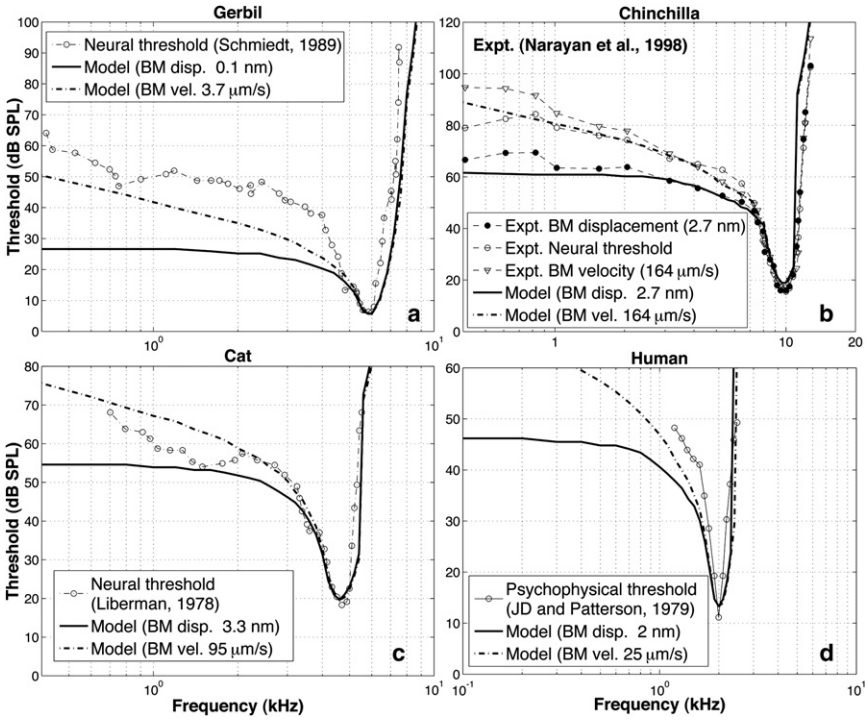

FIGURE 4 Comparisons of threshold measurements with BM isovelocity and isodisplacement tuning curve calculations. Measured gerbil (*a*), chinchilla (*b*), and cat (*c*) frequency-threshold tuning curves for one auditory nerve fiber (33–35), and a measured human (*d*) psychophysical tuning curve (36) (*open circles with thin dash-dotted lines*), are compared to corresponding BM isodisplacement (*heavy solid lines*) and isovelocity (*heavy dash-dotted lines*) mechanical tuning curve calculations. Details of the simulation parameters can be found in Tables 2 and 3.

TABLE 3 Push-pull gains (α) versus input SPL at the ear canal

Input sound pressure at the ear canal (dB SPL)	Gerbil	Chinchilla	Cat	Human
70~90	—	—	—	—
60~70	0.10	0.07	0.07	0.07
50~60	0.12	0.09	0.09	0.09
0~50	0.14	0.11	0.11	0.11

Values shown were used for the calculations in Fig. 4.

α decreases toward zero, which is the value for the passive case.

For the chinchilla cochlea (Fig. 4 *b*), both the simulated and measured BM isovibration tuning curves correspond to a displacement of 2.7 nm at the characteristic frequency, which at that frequency corresponds to a velocity of 164 μm/s. At frequencies between the BF and 1 kHz, both the simulated BM isodisplacement (Fig. 4 *b*, *thick solid line*) and BM isovelocity (Fig. 4 *b*, *dash-dotted line*) tuning curves show good agreement with their experimental measurements (Fig. 4 *b*, *solid circles* and *open triangles*, respectively). However, below 1 kHz the simulated BM isovelocity and isodisplacement tuning curves are ~5 dB SPL lower than the corresponding measurements. The experimental and simulation results indicate that the BM isovelocity (164 μm/s) corresponds more closely to the neural-tuning measurements (Fig. 4 *b*, *open circles*) than to the BM isodisplacement tuning measurements (2.7 nm).

The calculated BM isodisplacement tuning curves of gerbil, cat, and human cochleae are at 0.1 nm, 3.3 nm, and 2 nm, respectively, and the calculated BM isovelocity tuning curves are at 3.7 μm/s, 95 μm/s, and 25 μm/s, respectively. The BM isodisplacement tuning curve for gerbils is lower than that for the other species by 26–30 dB.

For the cat cochlea (Fig. 4 *c*), the neural-tuning measurement appears between the calculated BM isovelocity and isodisplacement tuning curves. However, the calculated BM isovelocity tuning curve shows generally better agreement with the neural threshold measurement, especially for frequencies below the BF. In human cochleae (Fig. 4 *d*), the calculated BM isovelocity tuning curve shows a better fit to the psychophysical measurement below the BF (Fig. 4 *d*, *open circles*) than does the calculated BM isodisplacement tuning curve.

Similarity of Q_{10} values across species in both experiment and simulation

To provide a more global view, Fig. 5 shows the experimentally measured sharpness of frequency tuning ("Q_{10}") of cochlear neurons (38) as a function of the BF for gerbil, chinchilla, and cat, as well as the predicted values based on human psychophysical tuning data (39) (Fig. 5, *dash-dotted lines*), compared with the corresponding sharpness calculations based on the modeled isovelocity tuning curves (Fig. 5, *solid lines*). The Q_{10} value is calculated by dividing the BF by the 10-dB bandwidth. The cochlear model parameters from Table 1 were used for both the Q_{10} calculations and the V_{BM} calculations.

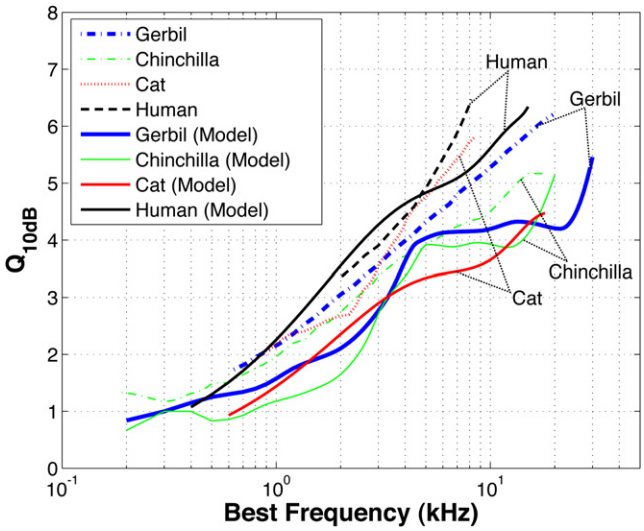

FIGURE 5 Comparison of frequency tuning sharpness (Q_{10}) between experimentally measured and model results, computed by dividing the BF by the 10-dB bandwidth. Q_{10} values based on cochlear neuron measurements for gerbil, chinchilla, and cat, as well as predicted Q_{10} values for human auditory-nerve-fiber frequency-threshold tuning curves (ANFTCs) (*dash-dotted lines*) are compared with model Q_{10} values based on computed isovelocity tuning curves (*solid lines*). Data for animals and humans are from Ruggero and Temchin (38).

With just a constant α gain factor along the BM in the model, Q_{10} values of the cochlear models show good agreement with experimental data within a factor of 2. Model calculations of Q_{10} across species generally show better agreement with experimental data in the low-frequency region than in the high-frequency region. The similarity of Q_{10} values across species is apparent in both the model and the experimental data, even though the dimensions of the auditory organs and the hearing bandwidths are very different. However, the Q_{10} value for the human V_{BM} tuning curve is higher than those for other animals by a factor of ~1.5–2 over the whole frequency region.

DISCUSSION

Basilar membrane motion

The BM relative velocity (V_{BM}/V_{ST}) calculation for the chinchilla cochlea (Fig. 3) shows generally better magnitude and phase agreement with the in vivo measurement (12) below the BF than does the gerbil cochlea (11), whereas above the BF, they both show comparable agreement with the in vivo data.

It is noted that significant differences exist when comparing $|V_{BM}/V_{ST}|$ across the two species. The gerbil $|V_{BM}/V_{ST}|$ is generally lower than that of the chinchilla by 15 dB for the passive case and by 28 dB for the active

case. This results in the lower BM isodisplacement and isovelocity values (0.1 nm and 3.7 μm/s) required to fit the gerbil neural-tuning curve at threshold (Fig. 4).

One often-stated reason for the lower $|V_{BM}/V_{ST}|$ measurements in gerbil is that surgically induced trauma in the experimental preparation results in a lower gain for the active case (40). However, this does not explain the lower response for the passive case of the gerbil cochlea. One reason for the relatively poor BM response for gerbil could be that the simple plate model used is consistent with measured anatomical values for the BM pectinate zone for chinchilla, cat, and human, whereas the gerbil actually has a (somewhat unique) two-layer pectinate zone with a pronounced arch in the collagen-fiber layer farthest from the OC (19) that has a substantially different mechanical behavior and is still under investigation at this time. For the calculations presented in this study, this equivalent flat plate model for the gerbil pectinate zone gives the correct cochlear map (Fig. S2). However, the thickness (Fig. 2 *b*) and collagen-fiber volume fraction (7) used in the model are not consistent with corresponding anatomical measurements for the gerbil cochlea. For the BM motion experiments, the arched BM likely leads to differences in the measured BM motion on the scala tympani side and the input to the IHCs. A more accurate model representation of the gerbil two-layer BM and OC anatomy will likely yield better agreement between simulation results and physiological measurements of the BM.

Neural thresholds

The neural-tuning threshold measurements for the four mammalian cochleae appear to be more closely related to the respective simulated BM isovelocity tuning curves than to the BM isodisplacement tuning curves (Fig. 4). This was also observed for measured BM isovelocity and isodisplacement tuning curves available for the guinea pig cochlea (41). It appears that the IHCs are more sensitive to BM velocity than to BM displacement, which is reasonable, since the stereocilia of the IHCs are not inserted into the tectorial membrane (TM) and thus are velocity detectors corresponding to a high-pass-filter-like response (41). However, the link between the IHC and the BM can be disrupted. This is illustrated in a report of a mouse mutant (42) in which the OHCs are normal and generate normal emissions but the TM is substantially modified, which causes a 60-dB loss in hearing. The Hensen's stripe, normally near the IHC, and the outer margin are missing. Thus, a proper TM is needed to deliver the BM motion to the IHC.

Typically, the modeled BM isovelocity tuning curves and measured neural thresholds are not entirely in agreement around half an octave or more below the BF, except in the chinchilla (Fig. 4). This may arise from the model's simple treatment of the middle ear as a single gain value for all frequencies, which tends to overstate the actual middle-ear gain at low frequencies. Another possible explanation is that no micromechanics of the OC were included in this model. Although the modeled BM isovibration tuning curves and measured auditory nerve fiber threshold curves appear similar to one another, a number of transduction processes could affect how the BM velocity excites the auditory nerve, including some combination of 1), the micromechanical interactions among the BM, the cellular structures in the OC, the tectorial membrane, and the subtectorial endolymph (43–45); and 2), the electrical processes of transduction and synaptic transmission of the IHCs (46,47).

High-frequency plateau

The question often arises in cochlear mechanics discussions of a plateau in BM motion phase and amplitude where the phase and amplitude no longer decrease monotonically above the BF. The plateau never appears in neural recordings but is common in measurements of basilar membrane motion (12,46,48). A phase plateau, but not an amplitude plateau, is evident in cochlear models with a nonphysical mass attached to the basilar membrane (50). However, in our calculations of the traveling wave with the 3-D viscous fluid and a realistic density for the basilar membrane, from Steele and Taber (10) to the work presented here, the phase plateau never appears. This yields the excellent agreement with neural recordings for high frequencies seen in Fig. 4. A possible explanation may come from recent work (51) that includes both the slow traveling wave and the fast compression wave. For the two-chambered box model used here, with symmetric scala vestibuli and scala tympani areas, the fast wave has exactly the same behavior in both scalae. The equal pressure on both surfaces causes zero displacement of the BM, so the fast wave is usually ignored unless detailed pressure measurements are considered (8). If the scala areas are not equal, however, the viscous shear corrections to the pressure wave in the two scalae are different. As a consequence, the pressure in each scala is slightly different, causing a displacement of the BM due to the fast wave. This yields a plateau in both amplitude and phase, without considering the various propagation modes that could be present due to the fluid regions of the OC. This asymmetric fast-wave pressure effect is most likely present in the cochlea.

Sharpness of tuning across species

As observed in the experimental data, the sharpness of the cochlear tuning curves (Fig. 5, Q_{10}) in the cochlear model shows relative uniformity across species, even given the substantial variations in cochlear structural dimensions such as BM length and OC microstructure, as well as differences in hearing frequency ranges. However, Q_{10} values of modeled BM velocity tuning curves exhibit deviations from

experimental measurements that approach a factor of 2 at some frequencies.

A feature of the plot in Fig. 5 is that the Q_{10} curves for the measurements increase smoothly and in general monotonically with frequency, whereas for the model calculations, the curves also increase monotonically with frequency, but not very smoothly. The smooth appearance in the measurements is due to regression-line fits to a large number of measurements for a given species (36,52). The model calculations are for a single prototypical representation of a given species, and thus, there is no averaging across parameters for that species. With this in mind, we can ask what gives rise to the model variation of Q_{10} as a function of frequency. One possibility is that there is a relationship between the width of the tuning curve (and thus of Q_{10}) and the local width of the basilar membrane. Fig. 2 *a* shows that the BM width with respect to BM position varies smoothly for human and cat, but has more curvature for gerbil and chinchilla. In Fig. 5, we see that the Q_{10} values also vary more smoothly for human and cat, whereas the Q_{10} values for gerbil and chinchilla have more curvature, supporting the hypothesis that basilar membrane tuning and basilar membrane width are correlated. It has been shown previously (53,54) that the BM width and the "equivalent rectangular spread", a measure of the excitation pattern width along the BM, are related to each other, and that the latter is in turn related to the "equivalent rectangular bandwidth". The BF divided by the equivalent rectangular bandwidth is an alternative measure of tuning to the Q_{10} value used in this study.

Frequency independence of the gain

In this formulation, it is assumed that the feed-forward gain, α_1, and the feed-backward gain, α_2, are constant and independent of frequency. The gains can be thought of as the product of two components: 1), mechanical-to-electrical transduction (MET), and 2), electrical-to-mechanical transduction (EMT). Model simulations of isolated OHCs suggest that they can generate high-frequency electromotile length changes and force production at frequencies $>$20 kHz (55) if the cell is provided with sufficient changes in its receptor potential. This assumption of the EMT component is thought to fall apart if one considers that the cell membrane of OHCs has capacitive behavior, which would tend to roll off the receptor potential, and thus, the active amplification capability of OHCs would diminish as the frequency increases above a few kHz (56,57). Spector et al. (58) show that piezoelectric coefficients and the strain to the membrane capacitance determine the limiting value of the decrease in receptor potential. Liu and Neely (59) alternatively suggest that if the receptor current is sensitive to the velocity of the reticular lamina, then the receptor potential does not roll off. In addition, active hair bundle motility can contribute to amplification in the MET pathway. It is also well established that for knockout mice lacking the prestin motor molecule, the cochlear amplifier, and thus hearing, is significantly compromised (60–62). The assumption is reasonable, therefore, that the OHC MET and EMT pathways are complementary, and that the product of the two transfer functions is approximately flat over the BF region.

CONCLUSION

The cochlear model described in this article, which incorporates the feed-forward and feed-backward behavior of the "Y"-shaped OC cytoarchitecture, appears to work well with relatively few free parameters, each of which has clear anatomical interpretations and physical values. The cochlear responses simulated were the stapes-to-BM-velocity transfer function, the BM isovelocity and isodisplacement tuning curves, and Q_{10} values of cochlear tuning sharpness. The model results were shown to be consistent with in vivo measurements across species, with some noted discrepancies. The gerbil cochlea appears to be different in that the BM response is lower than those of other animals studied. One assumption made throughout is that the product of the OHC MET and EMT pathways is approximately constant in the BF region.

Cochlear selectivity and sensitivity can be studied by using this model with the help of more accurate information on OC microstructural dimensions across species. This cochlear model can also be extended by including a more detailed treatment of OC micromechanics (63,64).

SUPPORTING MATERIAL

Additional methods, results, references, three figures, and two tables are available at http://www.biophysj.org/biophysj/supplemental/S0006-3495(10)01437-2.

We thank Peter M. Pinsky for technical discussions and Kevin N. O'Connor for extensive editing help.

This work was supported by a grant from the National Institute on Deafness and Other Communication Disorders of the National Institutes of Health (R01-DC007910).

REFERENCES

1. Brownell, W. E., C. R. Bader, …, Y. de Ribaupierre. 1985. Evoked mechanical responses of isolated cochlear outer hair cells. *Science.* 227:194–196.
2. Frank, G., W. Hemmert, and A. W. Gummer. 1999. Limiting dynamics of high-frequency electromechanical transduction of outer hair cells. *Proc. Natl. Acad. Sci. USA.* 96:4420–4425.
3. Voldrich, L. 1983. Experimental and topographical morphology in cochlear mechanics. *In* Cochlear Mechanics. Mechanics of Hearing. E. de Boer. and M. A. Viergever, editors. Delft University Press, Delft, The Netherlands. 163–167.
4. Steele, C. R., G. Baker, …, D. Zetes. 1993. Electro-mechanical models of the outer hair cell. *In* Biophysics of Hair Cell Sensory Systems.

H. Duifhuis, J. W. Horst, P. van Dijk, and S. M. van Netten, editors. World Scientific, Singapore. 207–215.

5. Geisler, C. D., and C. Sang. 1995. A cochlear model using feed-forward outer-hair-cell forces. *Hear. Res.* 86:132–146.
6. Wen, B., and K. Boahen. 2003. A linear cochlear model with active bi-directional coupling. *Proc. 25th Annu. Intl. Conf. IEEE Eng. Med. Biol. Soc., Cancun*. 2013–2016.
7. Lim, K. M., and C. R. Steele. 2002. A three-dimensional nonlinear active cochlear model analyzed by the WKB-numeric method. *Hear. Res.* 170:190–205.
8. Yoon, Y. J., S. Puria, and C. R. Steele. 2007. Intracochlear pressure and derived quantities from a three-dimensional model. *J. Acoust. Soc. Am.* 122:952–966.
9. Yoon, Y., S. Puria, and C. R. Steele. 2009. A cochlear model using the time-averaged Lagrangian and the push-pull mechanism in the organ of Corti. *J. Mech. Mater. Struct.* 4:977–986.
10. Steele, C. R., and L. A. Taber. 1979. Comparison of WKB calculations and experimental results for three-dimensional cochlear models. *J. Acoust. Soc. Am.* 65:1007–1018.
11. Ren, T., and A. L. Nuttall. 2001. Basilar membrane vibration in the basal turn of the sensitive gerbil cochlea. *Hear. Res.* 151:48–60.
12. Ruggero, M. A., N. C. Rich, …, L. Robles. 1997. Basilar-membrane responses to tones at the base of the chinchilla cochlea. *J. Acoust. Soc. Am.* 101:2151–2163.
13. Raphael, Y., M. Lenoir, …, R. Pujol. 1991. The sensory epithelium and its innervation in the mole rat cochlea. *J. Comp. Neurol.* 314:367–382.
14. Neely, S. T., and D. O. Kim. 1983. An active cochlear model showing sharp tuning and high sensitivity. *Hear. Res.* 9:123–130.
15. Zweig, G. 1991. Finding the impedance of the organ of Corti. *J. Acoust. Soc. Am.* 89:1229–1254.
16. Breneman, K. D., W. E. Brownell, and R. D. Rabbitt. 2009. Hair cell bundles: flexoelectric motors of the inner ear. *PLoS ONE.* 4:e5201.
17. Peng, A. W., and A. J. Ricci. 2010. Somatic motility and hair bundle mechanics, are both necessary for cochlear amplification? *Hear. Res.*, Epub ahead of print.
18. Dannhof, B. J., B. Roth, and V. Bruns. 1991. Length of hair cells as a measure of frequency representation in the mammalian inner ear? *Naturwissenschaften.* 78:570–573.
19. Edge, R. M., B. N. Evans, …, P. Dallos. 1998. Morphology of the unfixed cochlea. *Hear. Res.* 124:1–16.
20. Decraemer, W. F., O. de La Rochefoucauld, …, E. S. Olson. 2007. Scala vestibuli pressure and three-dimensional stapes velocity measured in direct succession in gerbil. *J. Acoust. Soc. Am.* 121:2774–2791.
21. Naidu, R. C., and D. C. Mountain. 2007. Basilar membrane tension calculations for the gerbil cochlea. *J. Acoust. Soc. Am.* 121:994–1002.
22. Puria, S., N. K. Kim, … C. R. Steele. 2008. Cochlear scala areas and basilar membrane (BM) width with the straight and the bent modiolus using micro computed tomography (μCT) imaging. *Prog. 31st Midwinter Res. Mtg. Assoc. Res. Otolaryngol.*, *Phoenix*. No. 631.
23. Dallos, P. 1970. Low-frequency auditory characteristics: species dependence. *J. Acoust. Soc. Am.* 48:489–499.
24. Eldredge, D. H., J. D. Miller, and B. A. Bohne. 1981. A frequency-position map for the chinchilla cochlea. *J. Acoust. Soc. Am.* 69:1091–1095.
25. Cabezudo, L. M. 1978. The ultrastructure of the basilar membrane in the cat. *Acta Otolaryngol.* 86:160–175.
26. Liberman, M. C. 1982. The cochlear frequency map for the cat: labeling auditory-nerve fibers of known characteristic frequency. *J. Acoust. Soc. Am.* 72:1441–1449.
27. Lynch, 3rd, T. J., V. Nedzelnitsky, and W. T. Peake. 1982. Input impedance of the cochlea in cat. *J. Acoust. Soc. Am.* 72:108–130.
28. Wever, E. G. 1949. Theory of Hearing. Wiley, New York.
29. Békésy, G. v. 1960. Theory of Hearing. AIP Press, New York.
30. Thorne, M., A. N. Salt, …, S. L. Gewalt. 1999. Cochlear fluid space dimensions for six species derived from reconstructions of three-dimensional magnetic resonance images. *Laryngoscope.* 109:1661–1668.
31. Aibara, R., J. T. Welsh, …, R. L. Goode. 2001. Human middle-ear sound transfer function and cochlear input impedance. *Hear. Res.* 152:100–109.
32. Olson, E. S. 2001. Intracochlear pressure measurements related to cochlear tuning. *J. Acoust. Soc. Am.* 110:349–367.
33. Narayan, S. S., A. N. Temchin, …, M. A. Ruggero. 1998. Frequency tuning of basilar membrane and auditory nerve fibers in the same cochleae. *Science.* 282:1882–1884.
34. Schmiedt, R. A. 1989. Spontaneous rates, thresholds and tuning of auditory-nerve fibers in the gerbil: comparisons to cat data. *Hear. Res.* 42:23–35.
35. Liberman, M. C. 1978. Auditory-nerve response from cats raised in a low-noise chamber. *J. Acoust. Soc. Am.* 63:442–455.
36. Johnson-Davies, D., and R. D. Patterson. 1979. Psychophysical tuning curves: restricting the listening band to the signal region. *J. Acoust. Soc. Am.* 65:765–770.
37. Karavitaki, K. D. 2002. Measurements and models of electrically-evoked motion in the gerbil organ of Corti. PhD thesis. Boston University, Boston, MA.
38. Ruggero, M. A., and A. N. Temchin. 2005. Unexceptional sharpness of frequency tuning in the human cochlea. *Proc. Natl. Acad. Sci. USA.* 102:18614–18619.
39. Greenwood, D. D. 1990. A cochlear frequency-position function for several species—29 years later. *J. Acoust. Soc. Am.* 87:2592–2605.
40. Overstreet, 3rd, E. H., A. N. Temchin, and M. A. Ruggero. 2002. Basilar membrane vibrations near the round window of the gerbil cochlea. *J. Assoc. Res. Otolaryngol.* 3:351–361.
41. Sellick, P. M., R. Patuzzi, and B. M. Johnstone. 1982. Measurement of basilar membrane motion in the guinea pig using the Mössbauer technique. *J. Acoust. Soc. Am.* 72:131–141.
42. Legan, P. K., V. A. Lukashkina, …, G. P. Richardson. 2005. A deafness mutation isolates a second role for the tectorial membrane in hearing. *Nat. Neurosci.* 8:1035–1042.
43. Zwislocki, J. J. 1986. Analysis of cochlear mechanics. *Hear. Res.* 22:155–169.
44. Freeman, D. M., and T. F. Weiss. 1990. Hydrodynamic forces on hair bundles at low frequencies. *Hear. Res.* 48:17–30.
45. Cheatham, M. A., and P. Dallos. 1998. The level dependence of response phase: observations from cochlear hair cells. *J. Acoust. Soc. Am.* 104:356–369.
46. Ruggero, M. A., L. Robles, and N. C. Rich. 1986. Cochlear microphonics and the initiation of spikes in the auditory nerve: correlation of single-unit data with neural and receptor potentials recorded from the round window. *J. Acoust. Soc. Am.* 79:1491–1498.
47. Russell, I. J., and P. M. Sellick. 1983. Low-frequency characteristics of intracellularly recorded receptor potentials in guinea-pig cochlear hair cells. *J. Physiol.* 338:179–206.
48. Rhode, W. S. 1971. Observations of the vibration of the basilar membrane in squirrel monkeys using the Mossbauer technique. *J. Acoust. Soc. Am.* 49:1218–1231.
49. Huang, S., and E. Olson. 2009. High frequency plateau in gerbil auditory nerve tuning curves. *Prog. 32nd Midwinter Res. Mtg. Assoc. Res. Otolaryngol. Baltimore*. No. 623.
50. Allen, J. B., and M. M. Sondhi. 1979. Cochlear macromechanics: time domain solutions. *J. Acoust. Soc. Am.* 66:123–132.
51. Steele, C. R., N. Kim, and S. Puria. 2008. Hook region represented in a cochlear model. *In* Concepts and Challenges in the Biophysics of Hearing. N. P. Cooper and D. T. Kemp, editors. World Scientific, Singapore.

52. Sokolich, W. G., R. P. Hamernik, …, R. A. Schmiedt. 1976. Inferred response polarities of cochlear hair cells. *J. Acoust. Soc. Am.* 59:963–974.

53. Fletcher, H. 1995. The ASA Edition of Speech and Hearing in Communication. Acoustical Society of America, Woodbury, NY.

54. Allen, J. B. 1996. Harvey Fletcher's role in the creation of communication acoustics. *J. Acoust. Soc. Am.* 99:1825–1839.

55. Tolomeo, J. A., and C. R. Steele. 1998. A dynamic model of outer hair cell motility including intracellular and extracellular fluid viscosity. *J. Acoust. Soc. Am.* 103:524–534.

56. Santos-Sacchi, J. 1992. On the frequency limit and phase of outer hair cell motility: effects of the membrane filter. *J. Neurosci.* 12:1906–1916.

57. Housley, G. D., and J. F. Ashmore. 1992. Ionic currents of outer hair cells isolated from the guinea-pig cochlea. *J. Physiol.* 448:73–98.

58. Spector, A. A., W. E. Brownell, and A. S. Popel. 2003. Effect of outer hair cell piezoelectricity on high-frequency receptor potentials. *J. Acoust. Soc. Am.* 113:453–461.

59. Liu, Y. W., and S. T. Neely. 2009. Outer hair cell electromechanical properties in a nonlinear piezoelectric model. *J. Acoust. Soc. Am.* 126:751–761.

60. Liberman, M. C., J. Gao, …, J. Zuo. 2002. Prestin is required for electromotility of the outer hair cell and for the cochlear amplifier. *Nature.* 419:300–304.

61. Cheatham, M. A., K. H. Huynh, …, P. Dallos. 2004. Cochlear function in Prestin knockout mice. *J. Physiol.* 560:821–830.

62. Dallos, P., X. Wu, …, J. Zuo. 2008. Prestin-based outer hair cell motility is necessary for mammalian cochlear amplification. *Neuron.* 58:333–339.

63. Steele, C. R., and S. Puria. 2005. Force on inner hair cell cilia. *Int. J. Solids Struct.* 42:5887–5904.

64. Nam, J. H., and R. Fettiplace. 2010. Force transmission in the organ of Corti micromachine. *Biophys. J.* 98:2813–2821.